nature physics

Article

https://doi.org/10.1038/s41567-023-02243-9

Non-affine atomic rearrangement of glasses through stress-induced structural anisotropy

In the format provided by the authors and unedited

Supplementary Information

Contents

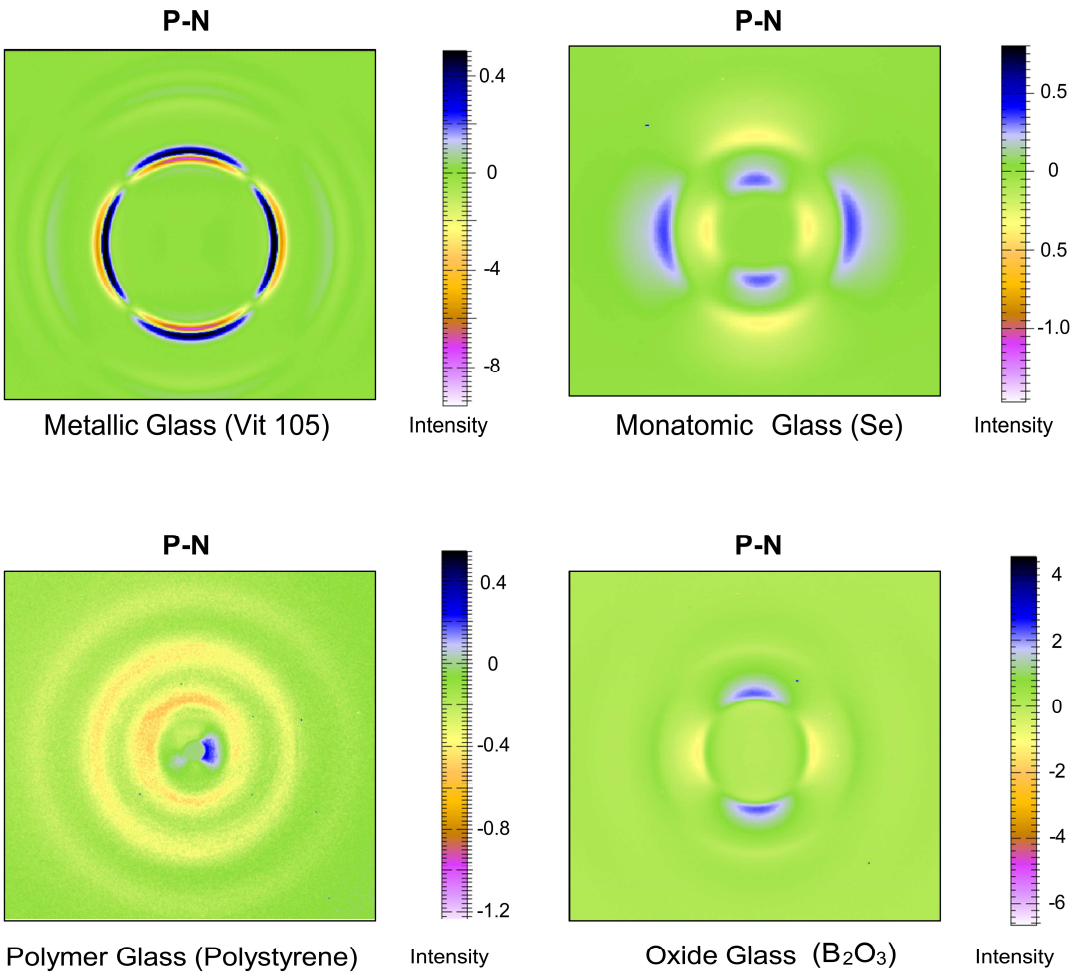

Figure S1. Signature of structural anisotropy in deformed glasses. After the high-temperature creep deformation, the nonoverlapped elliptical diffraction rings observed for various types of glasses, indicating an anisotropic structure.

Text SI. Error analysis for the higher-order terms in the calculation of $g_2^0(r)$

According to the perturbation expansions in Ref.41, the anisotropic PDF $g(\boldsymbol{r})$ under the uniaxial deformation is expressed in as:

$$g(\boldsymbol{r}) = g(r) + \frac{1}{n!}(-1)^{n-1}\left(\frac{1}{2}\right)^n \sum_{\alpha+\beta+\gamma=n} \frac{n!}{\alpha!\beta!\gamma!} \frac{\partial^n}{\partial x^\alpha y^\beta z^\gamma}[x^\alpha y^\beta (-2z)^\gamma \varepsilon^n(r) g(r)] \tag{S1}$$

Where $0 \le \alpha, \beta, \gamma \le n$, $\varepsilon(r)$ is the uniaxial strain. Specifically, for an affine compression strain, ε_{aff} along the z axis, the expressions of $g_2^0(r)$ for the first-order and second-order expansion can be directly obtained from **Eq. S1**:

For the first-order expansion:

$$g_2^0(r) = -\alpha r \frac{d}{dr} g(r) = -\alpha r \frac{d}{dr} g_0^0(r) \tag{S2}$$

For the second-order expansion:

$$g_2^0(r) = \frac{\sqrt{5}}{7}\alpha^2 r^2 \frac{d^2}{dr^2} g(r) + \left(\frac{17\sqrt{5}}{28}\alpha^2 - \alpha\right) r \frac{d}{dr} g(r) \tag{S3}$$

$$g_0^0(r) - g(r) = \frac{1}{2}\alpha^2 r^2 \frac{d^2}{dr^2} g(r) + \frac{13}{4}\alpha^2 r \frac{d}{dr} g(r) + \frac{15}{4}\alpha^2 g(r) \tag{S4}$$

Here, $\alpha = \varepsilon_{aff}/\sqrt{5}$ is taken as the fitting parameter. $g(r)$ and $g_0^0(r)$ are the isotropic PDF before and after deformation, respectively. For the first-order expansion, $g(r) = g_0^0(r)$, and for the second-order expansion, $g(r) \neq g_0^0(r)$ and their difference is given by **Eq. S4**. We also note that **Eq. 3** in our paper has the same form as **Eq. S1** if α is taken as $\frac{2(1+\nu)}{3\sqrt{5}}\varepsilon_{aff}$. Hence they play the equivalent role in fitting the experimental curves.

We then use **Eqs. S2** and **S3** to fit the experimentally observed $g_{2,exp}^0(r)$ to extract the part due to affine deformation, $g_{2,aff}^0(r)$. The fitting curves for the Vit105 metallic glass are shown as follows (**Fig. S2**). We can see that the curve of $g_{2,aff}^0(r)$ for the second-order expansion almost completely coincides with that for the

first-order expansion. The values of α for two fitted curves are 0.01005 and 0.01009, which are very close to each other. These evidences justify that the first-order expansion is accurate enough for extracting the affine part of $g_2^0(r)$ in our experimental analysis, and the higher-order terms can be neglected. In addition, we also calculated the $g_0^0(r)$ the curve for the second-order expansion, and it is also almost identical to the $g(r)$ curve, as shown in **Fig. S3**. This also verifies the validity of the first-order approximation from the other side.

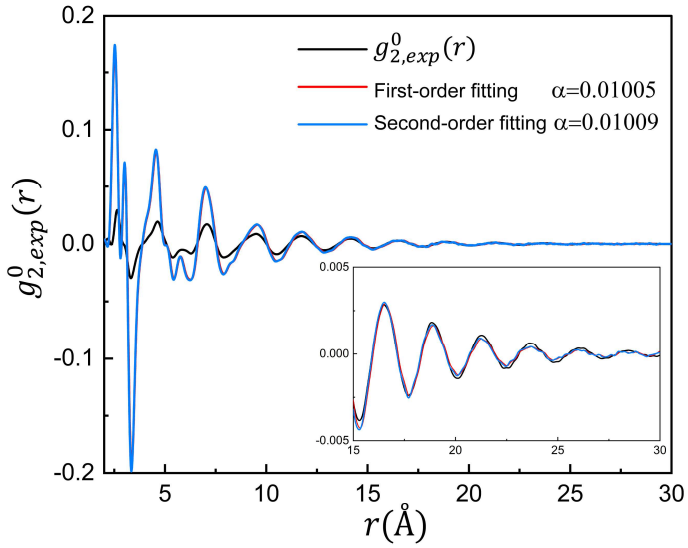

Figure S2. Comparison between the first- and the second-order approximation on extracting the affine part of anisotropic PDF. The theoretically fitted curves $g_{2,aff}^0(r)$ for the Vit105 MG according to the first-order and second-order expansion of $g_2^0(r)$, together with the experimentally observed $g_{2,exp}^0(r)$.

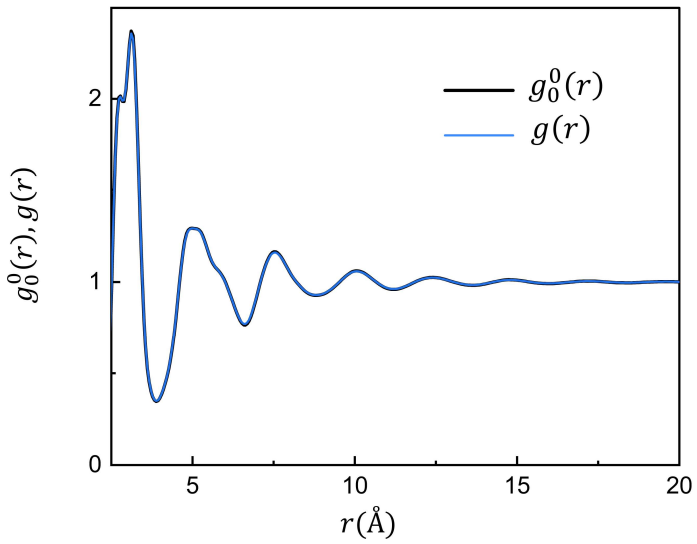

Figure S3. Comparison between the first-order approximation and original value of isotropic component of PDF. The calculated $g_0^0(r)$ curve for the second-order expansion, which is almost identical to the $g(r)$ curve, suggesting the validity of the first-order approximation.

Text SII. Determination of the radially varying nonaffine strain from experimentally measured PDFs

According to **Eq. S1**, we could also obtain the expression of $g_2^0(r)$ in the case of nonaffine strain for the first-order and second-order approximation, respectively:

$$g_2^0(r) = -\frac{1}{\sqrt{5}} r \frac{d}{dr}[\varepsilon(r) g(r)] \tag{S5}$$

$$g_2^0(r) = \left(\frac{1}{7\sqrt{5}} r^2 \frac{d^2}{dr^2} + \frac{17}{28\sqrt{5}} r \frac{d}{dr}\right)[\varepsilon^2(r) g(r)] - \frac{1}{\sqrt{5}} r \frac{d}{dr}[\varepsilon(r) g(r)] \tag{S6}$$

By solving the differential equations S5 and S6 with the experimental curves $g_{2,exp}^0(r)$ and $g_{exp}(r)$ of Vit105 MG, we obtain the spatially-dependent strain $\varepsilon(r)$ for the first-order and second-order approximation, respectively. The curves of $\varepsilon(r)$ obtained for the Vit105 MG are shown in **Fig. S4**. We can see that the curves of $\varepsilon(r)$ oscillate violently at small *r* and tend to approach a constant strain (affine) at large *r*, indicating that the nonaffine strain is spatially localized and tends to disappear for large distance *r*. In addition, we can also see that the strain curves $\varepsilon(r)$ for the

first-order approximation and second-order approximation almost overlap with each other. This again suggests that the first-order expansion is accurate enough for extracting the nonaffine strain and the higher-order terms can be neglected.

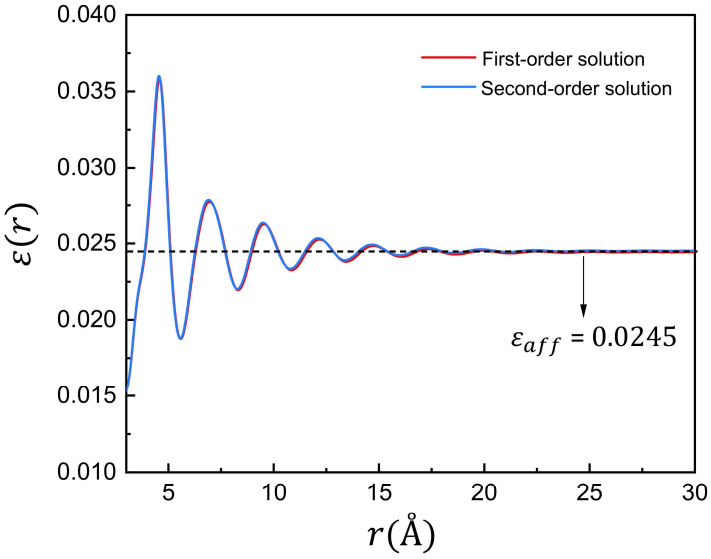

Figure S4. Comparison between the first- and the second-order approximation on extracting the nonaffine strain of anisotropic PDF. The spatially-dependent strain curves of $\varepsilon(r)$ solved from the experimental measured $g^0_{2,exp}(r)$ and $g_{exp}(r)$ of Vit105 MG for the first-order and second-order approximation, respectively.

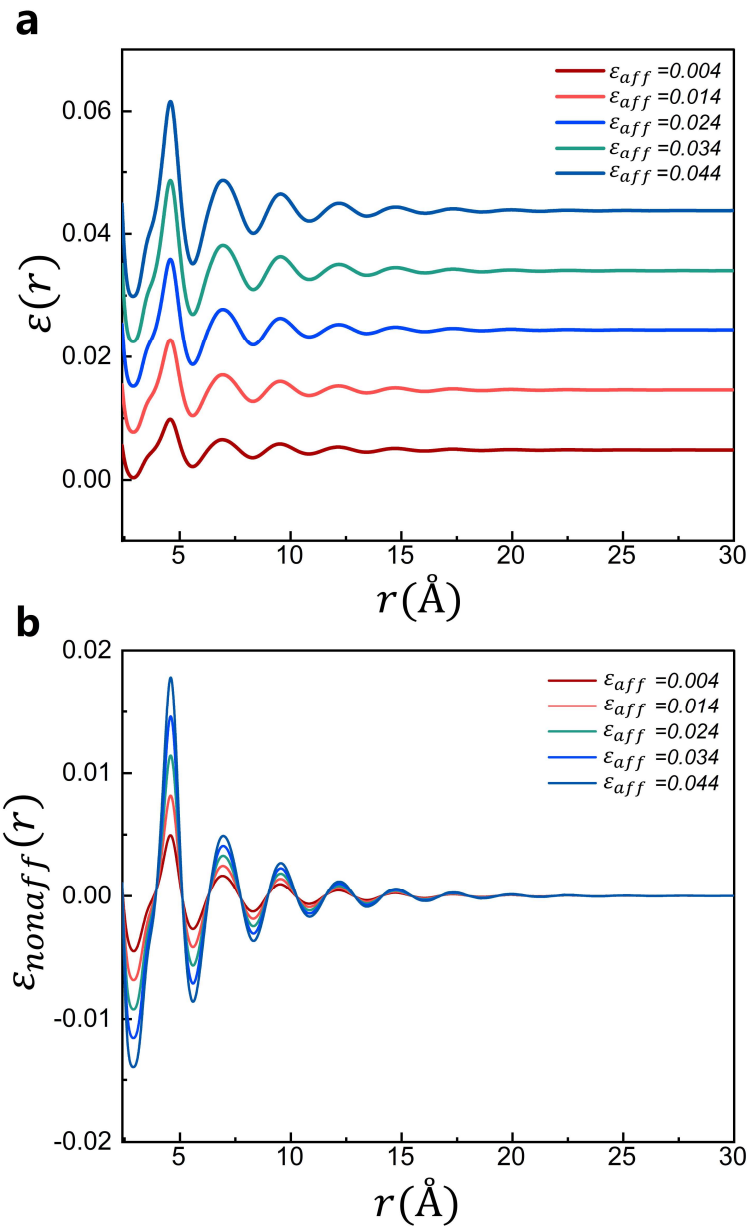

Figure S5. Correlation of the spatially dependent nonaffine strain with the constant affine strain. a, The calculated curves of the total strain $\varepsilon(r)$ for different values of the affine strain ε_{aff}. **b,** The extracted nonaffine strain curve of $\varepsilon_{nonaff}(r)$ for different values of affine strain ε_{aff}. The height of peaks of $\varepsilon_{nonaff}(r)$ are increased with ε_{aff}, while the peak positions are unchanged.

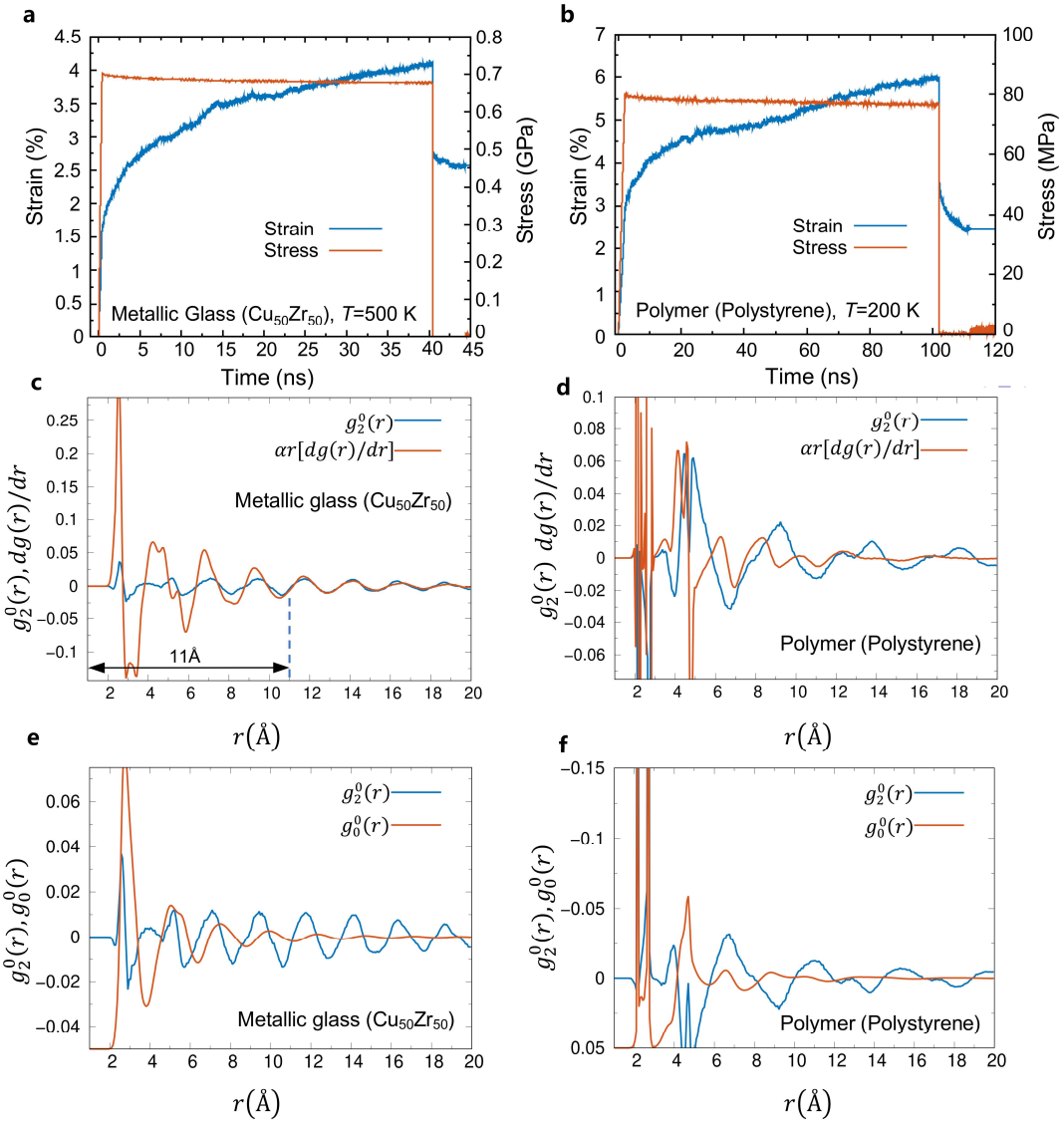

Figure S6. Simulated results for the metallic and polymer glasses. a and **b**, The stress-time curves during creep tests. **c** and **d**, The comparisons of anisotropic PDF $g_2^0(r)$ with the first deviation of isotropic PDF $\alpha r dg(r)/dr$. **e** and **f**, The comparisons of $g_2^0(r)$ with $g_0^0(r)$. The peak positions of the compared curves show a shift in the MG, whereas match well with each other in the polymer glass.

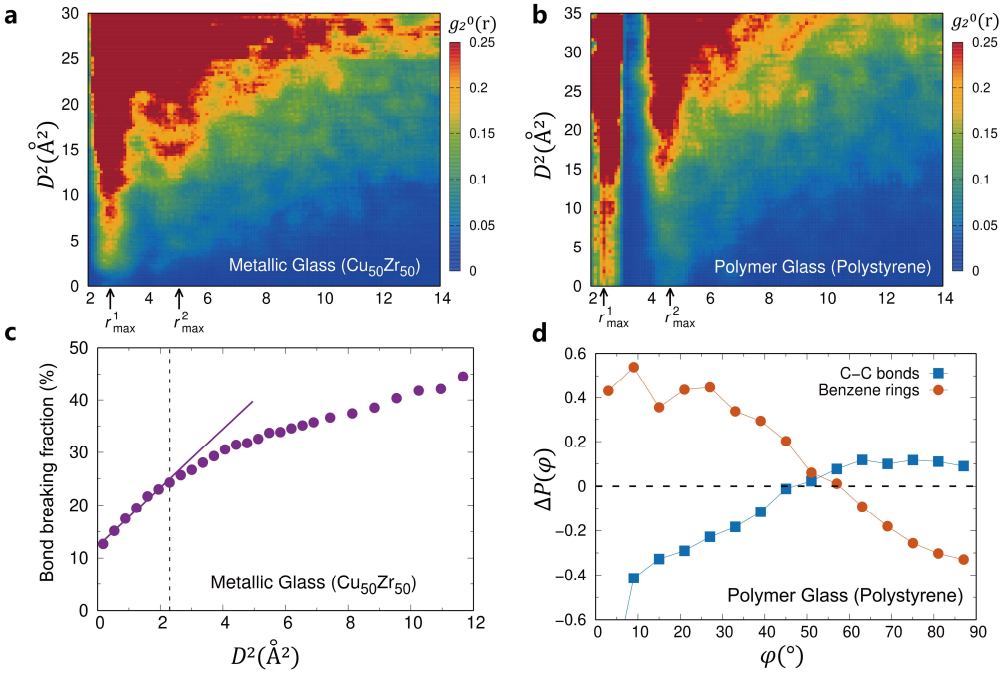

Figure S7. Correlations of structural anisotropy with nonaffine deformation and changes of bonds, by taking the cutoff of D^2 as 1.5 r_{min} in simulations, for the deformed metallic and polymer glasses. a and **b**, The intensity of $g_2^0(r)$ with the squared nonaffinity D^2 at any r, for both the MG and the polymer glass, respectively. **c,** In the MG, the variation of the fraction of the number of breaking bonds with D^2. **d,** For the polymer glass after creep, the dependence of angle probability distribution for the C-C bonds in aliphatic moiety and Benzene rings, respectively.

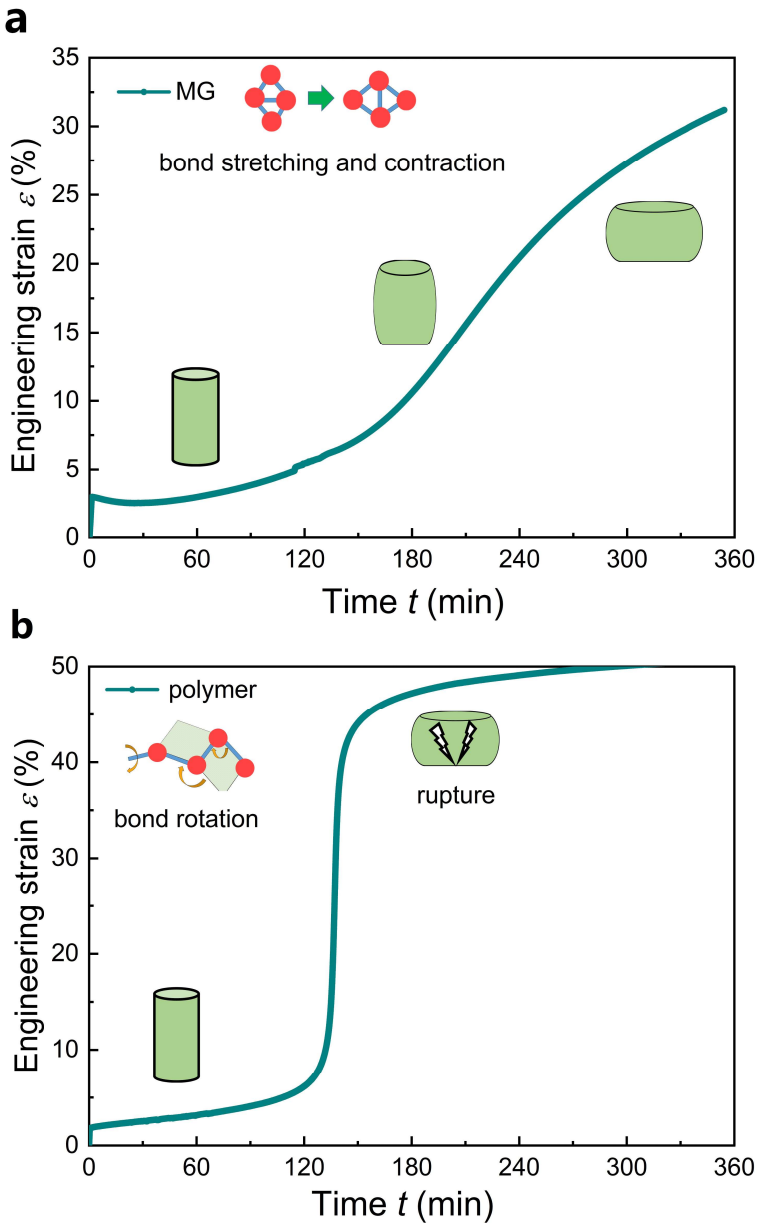

Figure S8. Correlation of the nonaffine mode of atomic rearrangements with macroscopic creep behavior for metallic and covalent bonded glasses. a, For the metallic glass with the nonaffine mode of the atomic bond stretching and contraction, the creep strain is increased gradually and continuously with the creep time; the sample was finally crept into a barrel shape without rupture. **b,** For the polymer glass with the nonaffine mode of atomic bond rotation, the creep strain increases sharply at some creep time in the later stage, indicating the rupture of the sample.

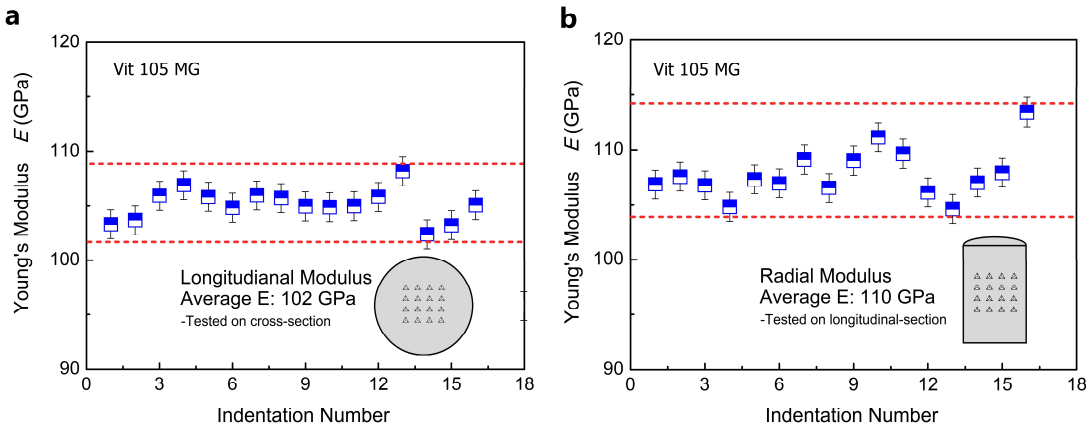

Figure S9. Modulus anisotropy in the deformed metallic glass. The modulus on the cross-section **a** and longitudinal section **b** of the crept Vit 105 MG, measured via the nanoindentation test. The averaged radial modulus is ~7.8% higher than the longitudinal modulus, indicating a mechanical anisotropy after creep.